Lidar observation of surface wind profiles in Changhua Coastal Industrial Park

Yuan-Shiang Tsai[1], Po-Hsing, Lin[2], Ya-Chao Yang[1], Jin-Lin Chen[3]
Taiwan Ocean Research Institute, NARL[1],
Department of Atmospheric Sciences, National Taiwan University[2]
Taiwan Power Company[3]

Abstract

The surface wind profiles and wind fluctuations were observed using a Lidar wind profiler in Changhua Coastal Industrial Park. The observation was independently conducted in each season with the measurement period of approximately one week. In the measurement site there were wind turbines. To prevent the contaminated data caused by turbines, the present analysis used four reference wind directions of NE, SSW, SE, and NW direction. The measurement results showed that two types of the profiles were observed. For the strong wind profiles caused by winter or summer monsoon, dominated by the surface friction, the wind speed increased and the turbulence intensity decreased with the increase of the height. In contrast, for the weak wind considerably affected by thermal buoyancy, the wind speed and turbulence profile was complex. Wind speed can decrease with the increase of the height. Turbulence intensity was higher and increased with the increase of height. Conventional curve of empirical power law well fitted all of the profiles of the wind speed and turbulence intensity with the height lower than 110 m. Discrepancy to the power law prediction was observed with the height over 110 m.

Key word: Surface boundary layer, atmospheric turbulence, wind power

1. Introduction

The wind observation using Light Detect and Ranging (Lidar) is an advanced remote sensing technology and in advantage of studying the surface atmospheric boundary layer (SABL). Particularly, the surface boundary layers below 200 meters have significant effect on the physical process of mass, momentum, and energy transfer from sea or land to the atmosphere, which substantially influences the regional weather and our living environments. In wind power deployment, this surface layer is located in the height of wind turbines. The vertical distribution of wind speed, wind direction, flow inclination, and wind fluctuations represented by turbulence intensity affects the power output (Wagner et al. 2008). Understanding the wind characteristics inside the rotor swept area is essential to account the turbine performance.

Conventionally, a meteorological mast is employed to observe the wind profile. However, few data are available to an altitude over 100 m (Tamura et. al 2007). This is because the difficulty to construct a very tall tower. Using Lidar to observe the SABL up to hundreds of meters has significantly progressed over the past few decades and applied in widespread fields. Pena et al. (2009) used a continuous-wave Lidar wind profiler to study offshore wind and turbulence for the assessment of wind characteristics utilized in wind power generation. Drew, Barlow, and Lane (2013) employed a pulsed Doppler Lidar to observe the urban boundary layer in high wind speed conditions. The wind speed profile was well fit the logarithmic relationship below 1000 m. Tse et al. (2013) observed the typhoon wind profile using both Lidar and Sodar and concluded that log-law and power-law reasonable estimates the profiles below 300 m.

Taiwan is located in the East Asia monsoon region. The wind shows a seasonal variety. In winter, the northeast monsoon is dominant and the strong wind gust is brought by cold fronts. In the summer, the prevailing wind is produced by the southwest monsoon. Besides, typhoons frequently invade the island in the summer and autumn with the extremely large wind speeds. In contrast, without the synoptic weather system, the wind is generally a diurnal cycle of the sea-land breeze, particularly significant in the coastal region. Tsai et al. (2013) conducted a preliminary study of the sea-land breeze observed using Lidar in the tidal land of Ganghua, showing that the wind from the seaside appeared to be a low level jet type when the wind speed was weak. However, it is noted that the detailed formation of SABL with various weather conditions has not yet been detailed studied in Taiwan.

In the current study, the observation of SABL was conducted using a portable WINDCUBE v2 Lidar with the measurement altitudes ranging from 43 to 210 m in Changhua Coastal Industry Park. Mean wind speed profile, turbulence intensity, flow inclination, and directional variations along with the vertical direction were examined with a variety of the reference wind speeds and directions. In addition, an empirical power-law was employed to fit the observed wind data. This is used to understand the characteristics of the wind profiles under different atmospheric conditions.

2. Lidar description

The Lidar employed in the present study was WINDCUBE v2, a pulsed Doppler Lidar, with the light wave length of 1543 nm for eye safety. This wind profiler emitted laser beams from five beam positions, one pointing to zenith while others incline to the zenith with 28 degrees. The radial velocities were observed along with the line-of-sight (LOS) by extracting returning signal scattered by atmospheric aerosols, which contained the information of the Doppler shift. Figure 1 explained the measurement orthogonal frame. The frame was directed to North. Laser beams scanned in the sequence of vertical, north, east, south, and west direction. From the geometry, the component of the wind velocity u, v in NS and EW direction was retrieved from the radial velocity as follows:

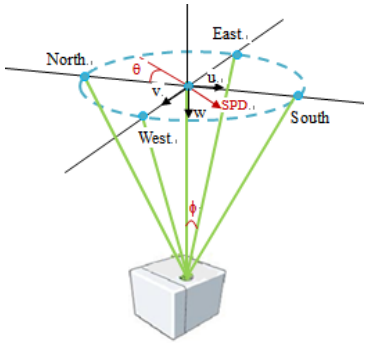

Figure 1 Orthogonal frame of the WINDCUBE V2 system

$$u = (Vr_N - Vr_S)/2sin\phi \quad (1)$$

$$v = (Vr_E - Vr_W)/2sin\phi \quad (2)$$

where Vr_N, Vr_S, Vr_E, and Vr_W represented the radial velocity in north, south, east, west, and vertical direction, respectively. Hence, the horizontal wind speed was denoted by U and wind direction was denoted by θ in the meteorological coordinate was as follows:

$$U = \sqrt{u^2 + v^2} \quad (3)$$

$$\theta = tan^{-1}(u/v) \quad (4)$$

The vertical velocity was directed obtain from the beam sent in zenith:

$$w = Vr_V \quad (5)$$

where Vr_V denoted raidal velocity in vertical direction.

The principle to measure the horizontal wind speed requires the assumption of horizontal homogeneity of the flow field. The assumption is reasonable for a flat terrain or offshore, but is limited for the measurement in complex terrain (Cariou 2011).

WINDCUBE adopted the Doppler Beam Swinging (DBS) method to obtain the wind data. This scan type with a shorten scan time was in advantage of measuring the unsteady wind experienced in the nature when compared with the Velocity Azimuth Display (VAD) as used in Pena et al. (2009). The duration between each beam measurement was approximately 0.7 seconds, depending on the effetness of the receving signal. Hence, a circle of scanning indicated the the time resolution of the measurements was approximate 3.5 seconds.

3. Measurement site and data processing

3.1 Site description

The measurement site was in Changhua Coastal Industry Park located in the coast of the middle-west Taiwan. The site was a reclaimed land apart from Taiwan Island with road connection in the north area as shown in the figure 2(a). This region is well-known for strong wind in the winter and hence wind turbines were constructed here. There were seven wind turbines located around the Lidar as depicted in figure 2(b) with numbers. The existence of wind turbines contaminated the wind flow, forming the wake behind the turbines. For the wind profiles affected by wind turbines were not considered in the present analysis.

(a)

(b)

Figure 2 (a) the measurement in Changhua Coastal Industry Park (b) detailed description the Lidar's location and the distance to surrounded wind turbines.

The wind Lidar was installed in the roof of the container with 3 m in height near the west seashore. The wind at 11 levels with the height of 43, 50, 60, 70, 90, 110, 130, 150, 170, 190, and 210 m respectively were observed. The observations were carried out approximately one week for each season independently. The four measurements were 24 to 31 Mar in spring, 23 to 30 June in summer, 22 to 29 Sep. in autumn, and 16 to 22 Dec. in winter, respectively. An meteorological mast, 70 m in height, instrumented with meteorological sensors in three levels, 30, 50, and 70 m respectively, located beside the Lidar was employed for one year observation to obtain meteorological parameters.

3.2 Data processing

Data manipulations were based on the mean value of 10-min datasets. According to the resolution of the

present Lidar measurement, each 10-min set had approximately 170 data points. The datasets with the availability more than 60% were recognized to be good quality. Here, the availability was defined as the number of valid data to the number of total data in 10-min. The valid data was quantified by the Carrier to Noise Ratio (CNR) value , which should be larger than the threshold of -23 as illustrated in the Windcube manual (Leoshpere 2012). Generally, the CNR value is determined by the concentration of aerosols in the atmosphere that backscatter laser light. High backscatter coefficient causes high CNR. The weather conditions affected the measurements. Aitken, Rhodes, and Lundquist (2012) concluded that the CNR value was linearly proportional to aerosol backscatter and was likely to be higher in the day than night. Precipitation affected the measurement performance because rainfall was measured instead of vertical wind speed. In the present measurements, Lidar was carried out under the circumstance without rainfall.

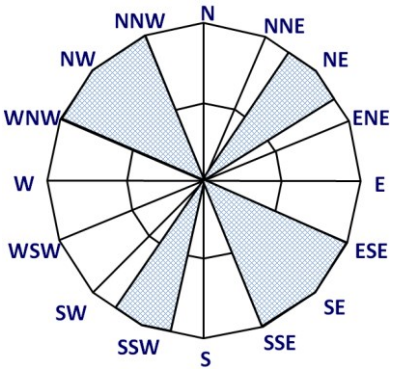

Figure 3 Analyzed wind data in the four directions to represent northeast moon, southwest moon, onshore wind, and offshore wind, respectively

Because wind was observed in four seasons, the inward directions may represent different atmospheric condition or seasonal variations. Also, the surface roughness was not equivalent when the wind came from different directions. This affected the formation of the SABL. Consequently, in analyzing the wind profile data were divided into 16 segments based on the reference wind direction θ_R. Besides, the profiles were categorized into groups according to the reference wind speed U_R with the bin size of 2 m/s. The reference wind direction and reference wind speed were the value by averaging all 11 altitudes. This prevented the "conditional ensemble averaging operation" as illustrated by Tamura et al. (2007). Ensemble averaged wind profile were made depending on θ_R and U_R.

The present study discussed the ver distribution of wind speed, turbulence intensity, flow inclination, and the discrepancy of wind direction. The empirical power law was used to fit the ensemble averaged profiles. The power law was described as follows:

$$U(z)/U_r = (z/z_r)^{\alpha} \quad (6)$$

$$TI(z)/TI_r = (z/z_r)^{\beta} \quad (7)$$

where z denoted the height; TI denoted turbulence intensity; U_r and TI_r denoted the wind speed and turbulence intensity at the reference height z_r; Here the reference height was the lowest observation point at 43 m. α and β are the power law exponent for the wind speed and turbulence intensity respectively. TI was defined as follows:

$$TI(z) = U_\sigma(z)/\bar{U}(z) \quad (9)$$

where $\bar{U}$ represented the mean wind speed in 10 minutes; U_σ represented the standard of the wind speed in 10-min. The flow inclination was represented by:

$$\Phi(z) = tan^{-1}(\bar{W}(z)/\bar{U}(z)) \quad (10)$$

where $\bar{W}$ represented mean vertical velocity. The vertical distribution of direction difference $\Delta\theta(z)$ was given as follows`:

$$\Delta\theta(z) = \theta(z) - \theta_r \quad (11)$$

where θ_r dented the wind direction observed at the 43 m.

Four reference wind directions, NE, SSW, NW, and SE, were used in the present analysis. These directions of wind were not contaminated by turbine wake effects. Because the samples for the NW and SSE wind were few, the bin sizes in these two directions were expanded as illustrated in figure 3. The wind characteristics in day and night may be various because the solar heating caused atmospheric stability. Consequently, the 10-min ensemble mean values were averaged for the day time except for the SE wind direction using night time data, because the wind blew for land to sea with the cooling effect at night.

4. Measurement results and discussion

4.1 Time series of wind speed and direction

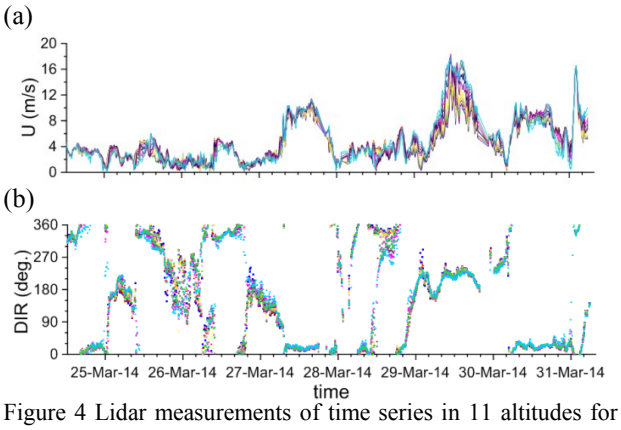

Figure 4 Lidar measurements of time series in 11 altitudes for (a) the wind speed and (b) the wind direction altitudes in spring. Caption: wind speed — 43 m; — 50 m; — 60 m; — 70 m; — 90 m; — 110 m; — 130 m; — 150 m; — 170 m; — 190 m; — 210 m; wind direction ● 43 m; ◆ 50 m; ▲ 60 m; ▲ 70 m; ✦ 90 m; ✖ 110 m; ▶ 130 m; ◆ 150 m; ★ 170 m; ⊕ 190 m; ▲ 210 m

Figure 4 demonstrated the Lidar measurement of the 10-min averaged horizontal wind speed and direction in all 11 altitudes in March. The majority of the wind was from NE direction. Occasionally, the wind direction changed to south or southeast. The wind speed was not strong when there were no synoptic events of cold fonts or hot fonts from northeast or southwest. The strong

southwest wind approximately up to 16 m/s was observed in 30 March. The variations showed the large deficient of the wind speed at different level of height. In contrast, large wind direction discrepancy was observed in 26 March under the conditions with very weak wind.

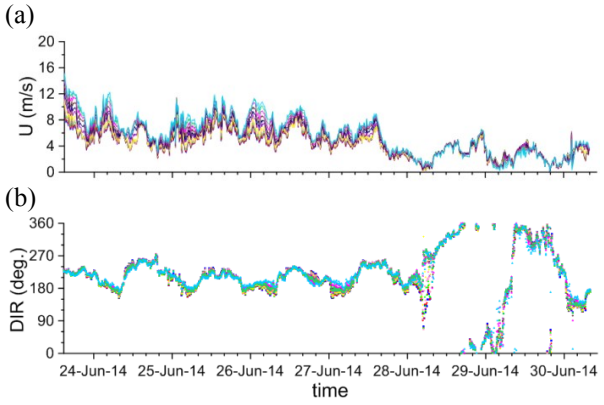

Figure 5 Lidar measurements of time series in 11 altitudes for (a) the wind speed and (b) the wind direction altitudes in summer. Caption was equivalent to figure 4

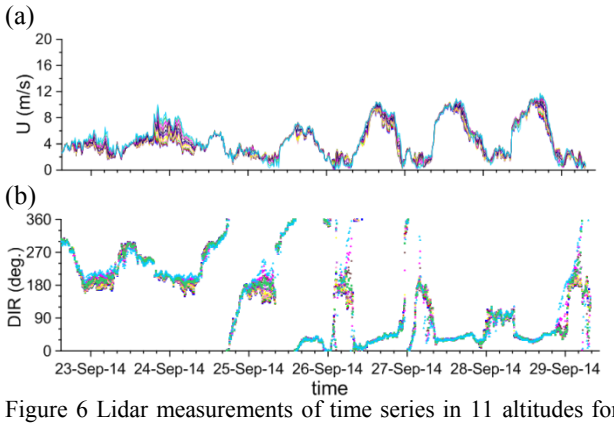

Figure 6 Lidar measurements of time series in 11 altitudes for (a) the wind speed and (b) the wind direction altitudes in autumn. Caption was equivalent to figure 4

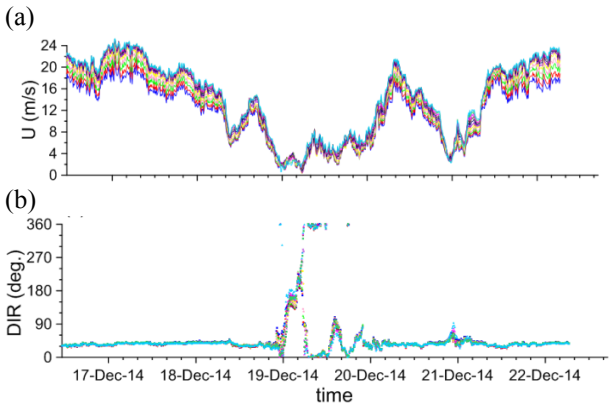

Figure 7 Lidar measurements of time series in 11 altitudes for (a) the wind speed and (b) the wind direction altitudes in winter. Caption was equivalent to figure 4

Figure 5 showed the variations of the wind speed and direction measured in June along with time. The wind speed in this period was generally weak. The wind directions varied from southwest in day to southeast at night during 23 to 28 in June. This regularly diurnal cycle was generated by the solar thermal effect. In the autumn observed in September as depicted in figure 6, the wind speed showed a distinctly diurnal cycle. The wind speed reached to the maximum value at midday. However, different from the direction variation in June, the wind direction was north in day but south at night. Figure 7 described the wind characteristics in December. The observation showed a large time-scale variation. It took two or three days to increase or decrease the wind speed. Generally, in winter the wind was northeast monsoon. The local wind speed was strong and up to 24 m/s. The wind direction was very steady except the occurrence of the weak wind speed.

4.2 distributions of vertical profiles

The vertical profiles of the mean wind speed in four reference wind direction of NE, SSW, NW, and SE were shown in figure 8 for each reference wind speed U_R. Tieleman (2008) explained that with a power exponent of 1/7 the appropriate range to agree with the power law distribution was between 20 and 100 m in height. Because the present wind profile revealed at least the lower 5 points showing a straight line in log-log scale the present study used the data observed between 43 and 110 to fit the power law.

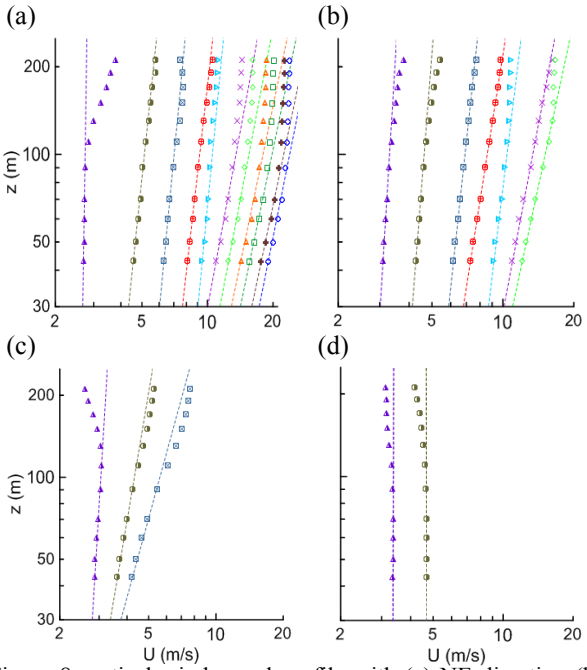

Figure 8 vertical wind speed profile with (a) NE direction (b) SSW direction (c) SE direction (d) NW direction. Captions: U_R=2-4 m/s; U_R=4-6 m/s; U_R=6-8 m/s; U_R=8-10 m/s; U_R=10-12 m/s; U_R=12-14 m/s; U_R=14-16 m/s; U_R=16-18 m/s; U_R=18-20 m/s; U_R=20-22 m/s; U_R=22-24 m/s. The dot line was the curve fitting using the power law.

For NE wind direction, strong wind speed basically representing the winter monsoon was observed. The power law index α was generally increased with the increase of U_R. The α value and number of samples n for

10-min ensemble averaging were given in Table 1. For the weak wind $2<U_R<4$ m/s, the wind speed significantly deviated from the power law over 110 m due to thermal convection effect. For the reference wind speed $4<U_R<12$ m/s, the profiles were in good agreement with power law to 210 m. However, with $U_R>12$, the observed profiles over 100 m gradually biased to a lower wind speed from the power law prediction.

Table 1 power law exponent α and number of 10-min samples n for ensemble averaging

	Reference wind direction θ_R			
U_R (m/s)	NE α (n)	SSW α (n)	NW α (n)	SE α (n)
2-4	0.020 (10)	0.075 (9)	0.003 (160)	0.073 (77)
4-6	0.140 (1)	0.096 (18)	-0.002 (78)	0.206 (11)
6-8	0.128 (23)	0.133 (30)	-	0.333 (1)
8-10	0.152 (43)	0.194 (14)	-	-
10-12	0.127 (9)	0.150 (1)	-	-
12-14	0.249 (14)	0.234(2)	-	-
14-16	0.254 (9)	0.264(5)	-	-
16-18	0.278 (42)	-	-	-
18-20	0.278 (38)	-	-	-
20-22	0.280 (18)	-	-	-
22-24	0.268 (9)	-	-	-

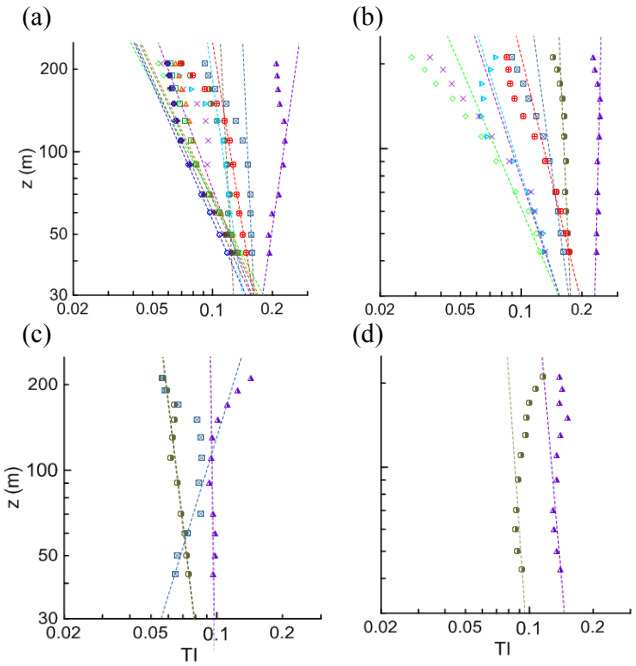

Figure 9 vertical profiles of turbulence intensity with (a) NE direction (b) SSW direction (c) SE direction (d) NW direction. Captions were equivalent to figure 8. The dot line was the curve fitting using the power law.

NW wind showed a medium wind speed. In the week wind $2<U_R<6$ m/s, the wind speed over 110 m deviated to a higher value when compared with the power law. However, for the strong wind $14<U_R<16$ m/s, the profile was analogous to the NE wind. The wind speed had lower value than power law curve in the higher altitudes. For the wind speed profiles from NW and SSE directions shown in figure 9 (c) and (d), their formation was induced by the sea-land breeze. This thermal buoyancy generated wind was generally weak. With the offshore wind blowing from land the profile had larger gradient. The particular wind profiles were observed in onshore wind blowing from the sea, the wind speed decreased with the increase of the height, which were different from a conventional boundary layer.

Vertical profiles of turbulence intensity in four reference wind directions were given in figure 9. It is apparent that for the reference wind speed of 2-4 m/s the turbulence intensities were larger than those of the higher U_R, at all levels. It may be explained that in the lower wind speed the thermal effects became stronger and hence generated buoyant turbulence. However, this effect decreased with the increase of U_R and hence reduced the turbulence intensity. Except $2<U_R<4$ m/s in NE direction, the turbulence decreased with the increase of the height. For $U_R>14$ m/s, the power exponent β had a value approximately to be -0.6. It was noted that for the height more than 100 m, the turbulence intensity gradient had a higher value than β fitted from the lower 5 points.

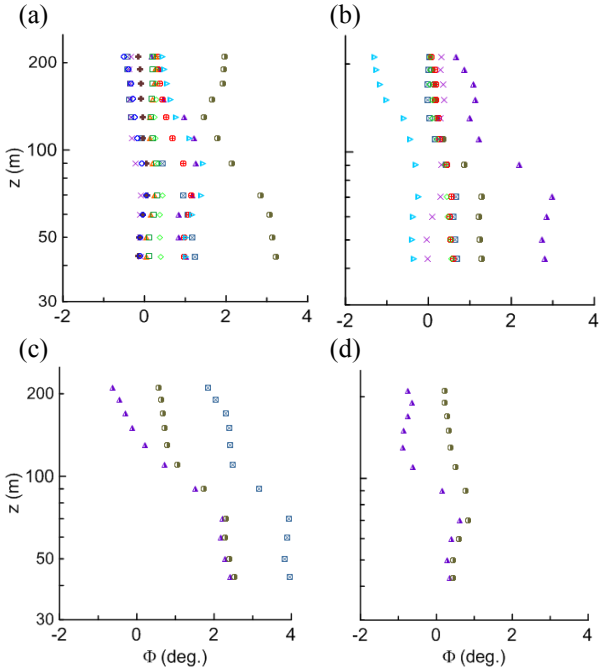

Figure 10 Vertical profiles of the flow inclination,Φ, with (a) NE direction (b) SSW direction (c) SE direction (d) NW direction. Captions were equivalent to figure 8.

The profiles of mean inclination were demonstrated in figure 10. For the present observation site with flat terrain, the inclinations were generally small and less than 4 degrees. The angles decreased with the increase of the height. Negative angles were observed particular for the SSW wind with U_R of 10-12 m/s, indicating the downwards flow of the winds.

Figure 11 demonstrated the profiles of directional difference in four reference directions along with the perpendicular direction. Tamura et al. (1999) studied the SABL using the Doppler Sodar. They found that the wind direction varied clockwise along with the vertical height. This agreed with the Ekman Spiral rotation caused by Coriolis force. For NE and SSW wind, the directional variations were small. However, some of the

profiles rotated counterclockwise disagreement with the Ekman Spiral direction. For SE and NW wind of the land-sea breeze, the thermal convection dominated and caused the significant directional variations. With the wind blowing from the land, the wind rotated clockwise along with the altitudes. In contrast, with the wind blowing from the sea, the wind directions varied counterclockwise. The largest directional difference was approximately -30 degrees, occurring for the onshore wind with $2<U_R<4$ m/s. Large directional variations were observed for NE wind with $2<U_R<4$ m/s, also indicating the strong thermal convection effects.

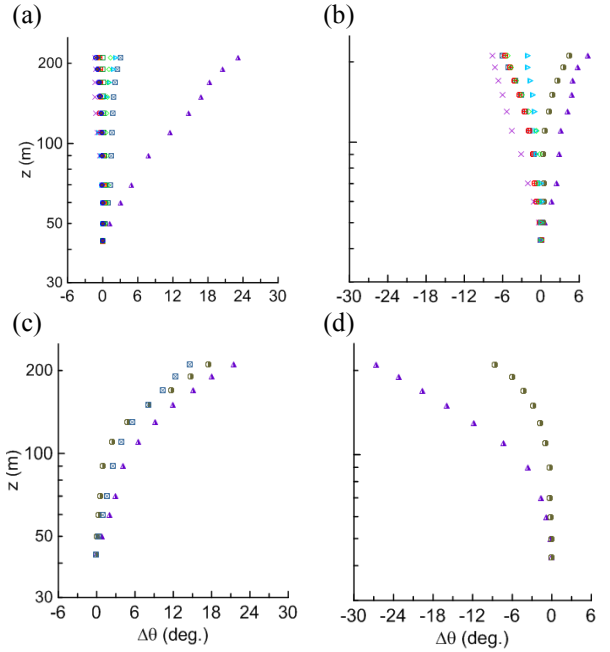

Figure 11 vertical profiles of the directional difference, Δθ, with (a) NE direction (b) SSW direction (c) SE direction (d) NW direction. Captions were equivalent to figure 8.

5. Conclusions

Near surface atmospheric boundary layer was observed using a Lidar wind profiler with the altitudes ranging from 43 to 210 m in Changhua Coastal Industry Park. Measurement results showed that no matter the reference wind speed U_R and direction θ_R and the atmospheric circumstance with or without the thermal effects, the power law was very well to describe the distribution of the wind speed with the height lower than 110 m. With the strong wind (U_R >12 m/s) in NE and SSW direction the observed wind speed profiles gradually deviated from the power curve and had a lower values than the power law prediction.

The turbulence intensity profiles showed that TI decreased with the altitudes. The power law was in good agreement with the observations under the height of 110 m. Flow inclinations were no more than 4 degrees, which was not significant for the present flat terrain. Considerable directional variations along with height were observed in the low wind speed, particularly occurring in the sea-land breeze caused by the thermal convention. The rotation was clockwise for offshore wind, however, counterclockwise for the onshore wind.

Reference

Cariou, J. P., 2011, "Pulsed lidars," in Remote Sensing for Wind Energy. Risøreport Risø-I-3184(EN). Ed. A Pena and C B Hasager, pp. 65–81.

Drew, D. R., Barlow, J. F., and Lane, S. E., 2013, Observations of wind speed profiles over Greater London, UK, using a Doppler lidar, Journal of Wind Engineering and industrial aerodynamics, **121**, 98-105.

Leosphere, 2012, WINDCUBE v2 Lidar remote sensor, User Manual.

Peña, A., Hasager, C. B., Gryning, S., Courtney, M., Antoniou, I., and Torben, M., 2009, Offshore wind profiling using light detection and ranging measurements, Wind Energy, 12, 105-124.

Tamura, Y., Iwatani, Y., Hibi, K., Suda, K., Nakamura, O., Maruyama, T., and Ishibashi, R., 2007, Profiles of mean wind speeds and vertical turbulence intensities measured at seashore and two inland sites using Doppler sodars, Journal of Wind Engineering and industrial aerodynamics, **95**, 411-427.

Tamura, Y., Suda, K., Sasaki, A., Iwatani, Y., Fujii, K., Hibi, K., and Ishibashi, R., 2007, Wind speed profiles measured over ground using Doppler sodars, Journal of Wind Engineering and industrial aerodynamics, **83**, 83-93.

Tse, K. E., Li, S. W., Chan, P. W., Mok, H. Y., and Weerasuriya, A. U., 2013, Wind profile observations in tropical cyclone events using wind-profilers and Doppler SODARs, Journal of Wind Engineering and industrial aerodynamics, **115**, 93-103.

Tsai, Y. S., Wu, C., Li, C., Lin, P. H., 2013, Intertidal zone wind profiling using Lidar measurement, Proceedings of 35rd Ocean Engineering Conference, Gaohsiung, Taiwan.

Tieleman H. W., 2008, Strong wind observation in the atmospheric surface layer, Journal of Wind Engineering and industrial aerodynamics, **96**, 41-77.

Wagner, R., Antoniou, I., Pedersen, S. M., Courtney, M. S., and Jørgensen, H. E., 2008, The influence of the wind speed profile on wind turbine performance measurements, Wind Energy, **12**, 349-362.